

## **Numerical modelling of flushing waves in sewer channels.**

Modélisation numérique des chasses hydrauliques dans les réseaux d'assainissement

Kamal El kadi Abderrezzak and André Paquier

Cemagref, Unité de Recherche Hydrologie-Hydraulique

3 bis quai Chauveau CP220 69336 Lyon Cedex 09 France

[elkadi@lyon.cemagref.fr](mailto:elkadi@lyon.cemagref.fr), [paquier@lyon.cemagref.fr](mailto:paquier@lyon.cemagref.fr)

### **RESUME**

Cet article présente les résultats d'une modélisation numérique du déplacement des dépôts de sédiment dans le réseau d'assainissement lors de lâchers d'eau. Un code de calcul mono-dimensionnel (1-D) est utilisé. Il repose sur les équations de Saint-Venant pour l'écoulement, l'équation d'Exner pour la continuité sédimentaire, et une loi de chargement introduisant un retard spatial du flux solide par rapport à sa valeur à l'équilibre. Ces équations sont résolues de façon couplée par un schéma explicite aux différences finies. Le modèle est testé sur le collecteur Tobelem à Marseille. Les résultats montrent que le modèle reproduit correctement les mesures.

### **ABSTRACT**

The present paper reports the results of a numerical investigation on the removal of sediment deposits in sewer system upon release of water from flushing device. A one-dimensional (1-D) model is built upon the de Saint-Venant equations for flow, the Exner equation for sediment continuity and a spatial lag equation for the non-equilibrium sediment transport. These governing equations are solved in coupled way by using a finite difference explicit scheme. The model is applied to data derived from the Tobelem sewer in Marseille. The numerical results show reasonably agreement with the available measurements.

### **KEYWORDS**

Flushing, One-dimensional model, Numerical modelling, Sediment transport, Sewer.

## 1 INTRODUCTION

Over the recent decades, there have been considerable efforts to improve the understanding of the efficiency of flushing operations in sewer system (Tait *et al.*, 2003, Guo *et al.*, 2004, Bertrand-Krajewski *et al.*, 2003, 2004). On the other hand, it is clear that there is a need for tools to predict the rate and magnitude by which sediment is removed from following flushing wave, where this sediment is deposited downstream and how it influences sewer bed morphology. Following the same evolution as in river modelling, the use of numerical models for the simulation of flushing waves has become an important part of water management strategy (Paquier *et al.*, 1997, Campisano *et al.*, 2004, 2006, Bertrand-Krajewski *et al.*, 2005).

In this context, the present paper reports the results of a numerical investigation on the sediment transport in sewer system upon release of water from flushing device. The coupled and non-equilibrium sediment transport approaches are used by the one-dimensional (1-D) model that is described in this paper. The model is used to simulate the scouring event that was recorded in the Tobelem collector in Marseille in response to flushing waves. The numerical results are compared to available measurements in order to assess the applicability and performance of the model.

## 2 MODEL DESCRIPTION

In this paper, attention is restricted to 1-D flow with uniform bed material represented by the median diameter  $D_{50}$ . The lateral inflows and outflows are neglected.

### 2.1 Governing equations

The governing equations for water flows are the 1-D de Saint-Venant equations

$$\frac{\partial \varphi}{\partial t} + \frac{\partial F(\varphi)}{\partial x} = G(x, \varphi) \quad (1)$$

$$\varphi = \begin{cases} S \\ Q \end{cases} \quad F(x, \varphi) = \begin{cases} Q \\ \frac{Q^2}{S} + P \end{cases} \quad G(x, \varphi) = \begin{cases} 0 \\ -gS \frac{\partial Z_b}{\partial x} - g \frac{Q|Q|}{K^2 S R^{4/3}} + B \end{cases}$$

where  $t$  = time;  $x$  = longitudinal distance;  $S$  = wetted area;  $Q$  = flow discharge;  $Z_b$  = bed elevation;  $g$  = gravitational acceleration;  $R$  = hydraulic radius;  $K$  = Strickler's coefficient;  $P = \int_0^h g(h-z)L(x,z)dz$  = hydrostatic pressure force;  $B = \int_0^h g(h-z) \frac{\partial L}{\partial x} dz$  = pressure force due to longitudinal width variation,  $h$  = water depth;  $L$  = channel width.

The sediment continuity is written in the terms of the Exner equation

$$(1-p) \frac{\partial A_s}{\partial t} + \frac{\partial Q_s}{\partial x} = 0 \quad (2)$$

where  $A_s$  = bed-material area;  $Q_s$  = volumetric sediment discharge;  $p$  = porosity.

### Non-equilibrium sediment transport equation

The model assumes a lag distance ( $D_{char}$ ) between the actual sediment transport rate  $Q_s$  and the sediment transport capacity  $Q_s^{cap}$  (Daubert and Lebreton, 1967).

$$\frac{\partial Q_s}{\partial x} = \frac{Q_s^{cap} - Q_s}{D_{char}} \quad (3)$$

The Meyer-Peter and Müller (1948) formula is selected for computing  $Q_s^{cap}$ . This formula has been widely used in the prediction of sediment transport in sewer channels (Bertrand-Krajewski *et al.*, 1993, Ashley and Verbanck, 1996).

### 2.2 Sediment modelling system

Inside one cell, four compartments are distinguished (Figure 1): a compartment  $I_n$  of input sediments and a compartment  $O_u$  of output sediments, referring to the particles that are routed downstream with water flow; a compartment  $A_c$  of the active layer; and one or several compartments ( $B_1, B_2, \dots$ ) composing the channel bed substrate. Sediment particles of each compartment are characterised by  $D = D_{50}$  and the mass  $M$ . Sediment exchanges between the compartments are computed in four steps:

1. part of the input sediment ( $Q_s^{tra}$ ) is transferred with flow to the output,
2. remaining part of the input sediment is deposited ( $Q_s^{dep}$ ) in the active layer;
3. particles are entrained from the active layer and exchanged with flow. This eroded part ( $Q_s^{ero}$ ) is mixed with particles travelling from input ( $Q_s^{tra}$ );
4. if the remaining part of the active layer mass is smaller than  $Q_s^{cap} \frac{\Delta x}{V}$ , then the bed is eroded. Thus, sediments go from the bottom to the active layer. Conversely, if the remaining part of the active layer mass exceeds  $Q_s^{cap} \frac{\Delta x}{V}$ , then deposition occurs and material is removed from the active layer and added to the bottom (layer  $B_1$  or creation of a new layer).

$$Q_s^{tra} = Q_s^{In} e^{-\frac{\Delta x}{D_{char}}} \quad (5)$$

$$Q_s^{ero} = Q_s^{cap} \left( 1 - e^{-\frac{\Delta x}{D_{char}}} \right) \quad (6)$$

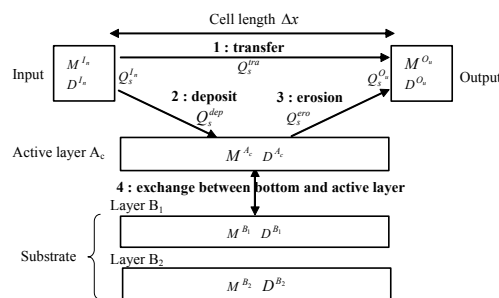


Figure 1. Representation of the sediment exchanges inside one cell (Balayn, 2001)

### 2.3 Numerical scheme

The set of equations (1) describes a system of hyperbolic conservation laws with source term ( $G$ ). The nonlinearity of the flux vector  $F$  may lead to spontaneous discontinuities in the case of flushing wave propagation. These discontinuities may have real physical meaning since the migration of the flushing wave includes steep

fronts, abrupt changes in flow rates and transitions between super- and sub-critical flows. Therefore, for the correct modelling of the flushing flow migration, a second-order Godunov-type explicit scheme is used. The main advantages of such scheme are that it is robust and able to solve the shallow water equations when large discontinuities between neighbouring points exist (Mingham and Causon, 1998).

In addition, the complete set of water and sediment transport governing equations is solved in a coupled procedure that includes the changes in bed elevation. The use of coupled techniques is supported by modellers as they eliminate the occurrence of numerical oscillations, handle rapid changes in boundary conditions, and are more stable than decoupled methods (Cao *et al.*, 2004).

The flow discharge  $Q$  and the wetted area  $S$  are computed at the middle of the hydraulic cell. The hydraulic cell is located between two cross-sections and given by the spatial interval  $[x_{i-1/2}; x_{i+1/2}]$ . The sediment cell is shifted by half a space step and given by the spatial interval  $[x_{i-1}; x_i]$ . Sediment discharge  $Q_s$  is computed in the middle of the hydraulic cell, and identified with respectively input and output of material in the sediment cell. Sediment transport capacity  $Q_s^{cap}$ , change in cross-section area  $A_s$  and bed elevation changes are computed in the middle of the sediment cell  $i$ , given by the cross-section located at  $x_{i-1/2}$ .

Hydraulic variables are computed in  $(x_i, t_n)$ ,  $i$  is space index denoting the location of the middle of the hydraulic cell  $i$ ,  $n$  is time index denoting a time level. The usual Courant-Friedrichs-Lewy condition is used for each hydraulic cell  $i$  in order to limit the time step. The numerical scheme includes five steps.

#### 1- Computation of $\varphi_{i-1/2}^n$ and $\varphi_{i+1/2}^n$

The slopes of  $Q$  and  $S$  are computed at time  $(x_i, t_n)$  by some kind of minmod relation.  $\varphi_{i-1/2}^n$  and  $\varphi_{i+1/2}^n$  are computed on the basis of these slopes. Two values are obtained for each variable:  $\varphi_{i-1/2l}^n$  and  $\varphi_{i-1/2r}^n$  obtained respectively from the cell  $i-1$  and the cell  $i$ , and  $\varphi_{i+1/2l}^n$  and  $\varphi_{i+1/2r}^n$  obtained respectively from the cell  $i$  and the cell  $i+1$  (indexes  $l$  and  $r$  mean respectively left and right side).

#### 2- Computation of $\varphi_{i-1/2}^{n+1/2}$

From a time discretization of Euler type on the hydraulic cell  $i$ , the values of  $\varphi$  are computed at time  $t_{n+1/2}$ . Two values are obtained for  $\varphi_{i-1/2}^{n+1/2}$ : one from the left cell  $i-1$  ( $\varphi_{i-1/2l}^{n+1/2}$ ) and one from the right cell  $i$  ( $\varphi_{i-1/2r}^{n+1/2}$ ).

#### 3- Resolution of the Riemann problem

As values at the same limit are generally different when computed from the left cell and from the right cell, a Riemann problem (with  $G = 0$ ) is considered and solved by using the Roe-type linearization (Roe, 1981). A unique value of  $\varphi_{i-1/2}^{n+1/2}$  is obtained.

#### 4- Sediment balance and cross-section shape updating at $t_{n+1/2}$

On the basis of the hydraulic variables calculated at  $t_{n+1/2}$ , the model computes the

sediment transport capacity  $Q_s^{cap}$  in the middle of each sediment cell. From equations 5 and 6 the sediment transport rate  $Q_{s_i}^{n+1/2}$  is calculated. Finally, change in cross-sectional area  $\Delta A_{s_{i-1/2}}^{n+1/2}$  is obtained from the continuity equation (2)

$$\Delta A_{s_{i-1/2}}^{n+1/2} = \frac{t_{n+1/2} - t_n}{1-p} \left[ \frac{(Q_{s_i}^{n+1/2} - Q_{s_{i-1}}^{n+1/2})}{x_i - x_{i-1}} + q_{s_{i-1}}^{n+1/2} \right] \quad (7)$$

This area change is applied to the cross-section by moving uniformly all section points below water level.

### 5- Computation of $\varphi_i^{n+1}$

The values at the middle of the hydraulic cell are computed in the new geometry from the difference of the fluxes for the conservative part of the equations and from an estimate  $G(x_i, \varphi_i^{n+1/2})$  of second member at time  $t_{n+1/2}$

$$\varphi_i^{n+1} = \varphi_i^n - \frac{\Delta t}{\Delta x} \left[ F(\varphi_{i+1/2}^{n+1/2}) - F(\varphi_{i-1/2}^{n+1/2}) \right] + \Delta t G(x_i, \varphi_i^{n+1/2}) \quad (8)$$

## 3 APPLICATION TO THE TOBELEM SEWER

A Hydrass gate was installed in the Tobelem collector in Marseille (France) in order to remove periodically the deposited material by flushing them downstream. At the end of May 1996, some measurements were performed by Balayn (1996).

The collector was composed of three straight reaches, with different longitudinal slopes: 2.6, 0.2 and 0.3% (Figure 2). The gate was positioned in the storage tank perpendicular to the flow and water was held behind. A sediment bed with initial uniform thickness of 0.15 m was deposited along the channel downstream of the gate. The bed material size ranged from 0.1 to 10 mm, with median diameter  $D_{50} = 2$ , density  $\rho_s = 2700 \text{ kg/m}^3$  and porosity  $p = 0.2$ .

Four gauges were installed along the collector to record the water levels and flow velocity attained during the flush waves of May 1996. Gauge  $H_{8.5m}$  was placed just downstream of the flush gate. Gauges  $H_{0m}$ ,  $H_{57m}$  and  $H_{115m}$  were located respectively 8.5m, 65.5 and 123.5 away from the flush gate. In addition, the location and thickness of the deposited material were measured after each of the 64 openings of the gate.

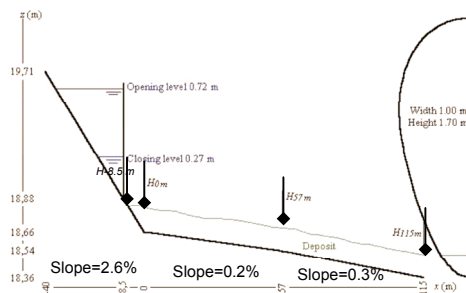


Figure 2. Longitudinal view of the Tobelem collector and location of measurements instruments

### 3.1 Model set up and boundary conditions

The part of the sewer located upstream of the gate is not modelled. The numerical simulation is conducted using  $\Delta x = 1$  m,  $D_{char} = 1.5$  m and  $K = 45$  m<sup>1/3</sup>/s. The time step  $\Delta t$  is determined as a function of the Courant number ( $C = 0.5$ ). A steady flow discharge of 0.005 m<sup>3</sup>/s corresponding to the mean leak discharge at the gate is used as initial condition. On the downstream side of the collector, the open boundary condition for the flow is assigned. To model the gate functioning during *one flush event*, a simple discharge hydrograph  $Q(t)$  and a limnigram  $h(t)$  are imposed at the gate location as upstream boundary conditions (Figure 3). The flow hydrograph is determined by considering the duration of the flush (25 seconds), the leak flow discharge (0.005 m<sup>3</sup>/s) and the peak discharge (0.305 m<sup>3</sup>/s) estimated on the basis of measurements at the gauge H-8.5m. Concerning the limnigram, the water depth is assumed to be constant and equal to 0.50 m (initial water depth in the storage tank) during the first eight seconds before decreasing progressively to 0.05 m.

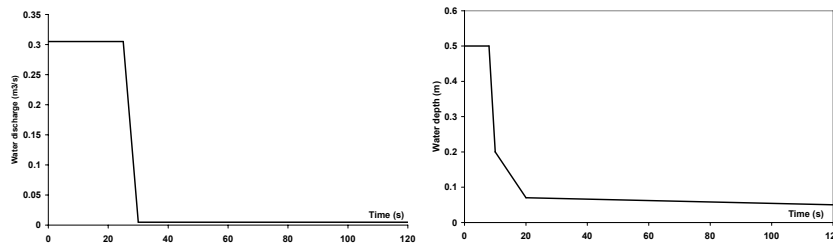


Figure 3. Upstream boundary conditions imposed at the gate location

These upstream boundary conditions are chosen in order to provide water levels that are as close as possible to measurements at least in the upstream part of the collector where erosion of sediments occurred. Figure 4 shows the comparison between the simulated and the measured limnigrams at  $H_{0m}$ ,  $H_{57m}$  and  $H_{115m}$ . The agreement between measurements and numerical results is seen to be acceptable. However, it is seen that the flush wave arrival is rather underpredicted by the model at  $H_{115m}$ . Two reasons could explain this discrepancy: the first one concerns some of the 1D de Saint-Venant hypothesis (small bottom slopes and curvatures, hydrostatic pressure and uniform velocity distribution in the cross-section, vertical velocity components neglected) that are violated almost locally during flushing operations (Cao *et al.*, 2004). The second one concerns the lateral inflows entering the collector between  $H_{57m}$  and  $H_{115m}$  that are not taken into account (Balayn, 2001). In the same way, changing the Strickler coefficient does not seem to improve the results without deteriorating the upstream results (sediment erosion, water level or velocity).

### 3.2 Results and discussion

The model is used to simulate the 64 openings of the gate. Figure 6 reports the simulated and measured sediment bed profiles. Globally, this figure points out that the simulated front position after each flush is in agreement with observations with a precision of 1 m corresponding to the space step adopted in the model grid. Moreover, it is seen that the model reproduces reasonably the form of the deposit bed at the end of each flush, with decreasing sediment heights of the deposit from upstream to downstream and the consequent advancing of the wavefront. Quite encouragingly, the model approaches the measured value of the sediment deposit height within a maximum error that does not exceed 3 cm (obtained at  $x=3$  m after 17

openings). Small differences between measured and simulated results are also observed elsewhere as the number of flushes increases.

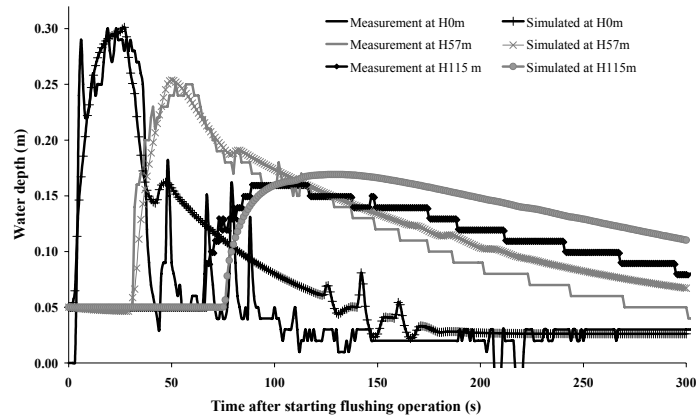


Figure 4. Water depth evolution at gauges H<sub>0m</sub>, H<sub>57m</sub> and H<sub>115m</sub>

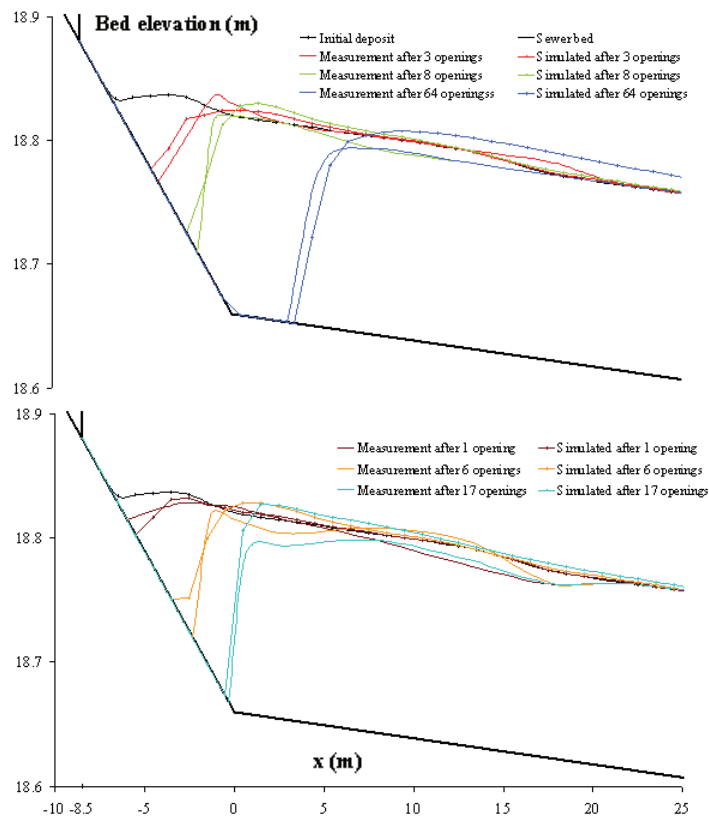


Figure 5. Comparison between measured and simulated sediment bed

## CONCLUSIONS

Flushing wave in sewer channels is studied from a coupled 1-D shallow water and non-equilibrium sediment transport model. In order to simulate accurately flushing operations and the associated steep fronts, abrupt changes in flow rates and transitions between sub- and super-critical flows, the second-order Godunov-type explicit scheme is used. The performance of the numerical model was investigated by comparing its predictions with field data derived from the Tobelem sewer collector in Marseille. Considering the small field scale, the degree of agreement between measurements and computational results was satisfactory. Indeed, although the model simplifies the complex physical process (particularly, the shallow-water approach, the two-phase flow assumption, hydrostatic pressure and uniform velocity distribution in the cross-section), the main aspects of the flushing wave were correctly reproduced. In addition, the sensitivity analysis of the numerical results to the lag distance, Strickler's coefficient and the sediment transport capacity formula was assessed but due to space limitations is not included here. Results highlighted the important role of these parameters. In particular, the influence of the Strickler's coefficient on the simulation of flushing wave seemed important and a strong need to take into consideration the variation of the roughness with time was identified.

## BIBLIOGRAPHIE

- Ashley, R.M. and Verbanck, M. (1996). Mechanics of sewer sediment erosion and transport. *JHR*, 34(6), 753-769.
- Balayn, P. (1996). *Modélisation du transfert de sédiments lors d'un lâcher d'eau en réseau d'assainissement : approche numérique* (in french). Université Louis Pasteur, Strasbourg.
- Balayn, P. (2001). *Contribution à la modélisation numérique de l'évolution morphologique des cours d'eau aménagés lors de crues* (in french). Université Claude Bernard Lyon 1. Lyon.
- Bertrand-Krajewski, J.L., Briat, P. and Scrivener, O. (1993). Sewer sediment production and transport modelling: a literature review. *JHR*, 31(4), 435-460.
- Bertrand-Krajewski, J.-L., Bardin, J.-P., Gibello, C. and Laplace, D. (2003). Hydraulics of a sewer flushing gate. *Wat. Sci. & Tech*, 47(4), 129-136.
- Bertrand-Krajewski, J.-L., Campisano, A.P., Creaco, E. and Modica, C. (2004). Experimental analysis on the hydraulic behaviour of flushing gates. *Proceeding of Novatech 2004*, Lyon.
- Bertrand-Krajewski, J.-L., Campisano, A.P., Creaco, E. and Modica, C. (2005). Experimental analysis of the Hydrass flushing gate and field validation of flush propagation modelling. *Wat. Sci. & Tech*, 51(2), 129-137.
- Campisano, A.P., Creaco, E. and Modica, C. (2004). Experimental and numerical analysis of the scouring effects of flushing waves on sediment deposits. *Journal of Hydrology*, 299, 24-334.
- Campisano, A.P., Creaco, E. and Modica, C. (2006). Experimental analysis of the Hydrass flushing gate and laboratory validation of flush propagation modelling. *Wat. Sci. & Tech*, 54(6-7), 101-108.
- Cao, Z., Pender, G., Wallis, S. and Carling, P.A. (2004). Computational dam-break hydraulics over erodible sediment bed. *JHR*, 130(7), 689-703.
- Daubert, A. and Lebreton, J.-C. (1967). Etude expérimentale sur modèle mathématique de quelques aspects des processus d'érosion des lits alluvionnaires, en régime permanent et non-permanent. *Proc. 12<sup>th</sup> IAHR congress*, Fort Collins, Colorado.
- Guo, Q., Fan, C., Raghaven, R. and Field, R. (2004). Gate and Vacuum Flushing of Sewer Sediment: Laboratory Testing. *JHE*, 130(5), 463-466.
- Meyer-Peter, E. and Müller, R. (1948). Formulas for bed-load transport. *Proc. 2<sup>nd</sup> IAHR congress*. Stockholm.
- Mingham, C.G. and Causon, D.M. (1998). High-resolution finite-volume method for shallow water flows. *JHE*, 124(6): 605-614.
- Paquier, A., Balayn, P. and Gendreau, N. (1997). A model for river morphology and sewer network. *Proc. 27<sup>th</sup> IAHR congress*, San Francisco.
- Tait, S.J., Chebbo, G., Skipworth, P.J., Ahyerre, M. and Saul, A.J. (2003). Modeling in-sewer deposit erosion to predict sewer flow quality. *JHE*, 129(4), 316-324.
- Roe, P.L., 1981. Approximate Riemann solvers, parameter vectors and difference schemes. *Journal of Computational Physics*, 43, 357-372.